Lab on a Chip

Cite this: *Lab Chip*, 2012, **12**, 1987–1994

www.rsc.org/loc

PAPER

Nanophotonic lab-on-a-chip platforms including novel bimodal interferometers, microfluidics and grating couplers†‡

Daphné Duval,[a] Ana Belén González-Guerrero,[a] Stefania Dante,[a] Johann Osmond,[b] Rosa Monge,[c] Luis J. Fernández,[c] Kirill E. Zinoviev,[d] Carlos Domínguez[d] and Laura M. Lechuga*[a]

Received 11th January 2012, Accepted 3rd April 2012
DOI: 10.1039/c2lc40054e

One of the main limitations for achieving truly lab-on-a-chip (LOC) devices for point-of-care diagnosis is the incorporation of the ''on-chip'' detection. Indeed, most of the state-of-the-art LOC devices usually require complex read-out instrumentation, losing the main advantages of portability and simplicity. In this context, we present our last advances towards the achievement of a portable and label-free LOC platform with highly sensitive ''on-chip'' detection by using nanophotonic biosensors. Bimodal waveguide interferometers fabricated by standard silicon processes have been integrated with sub-micronic grating couplers for efficient light in-coupling, showing a phase resolution of $6.6 \times 10^{-4} \times 2\pi$ rad and a limit of detection of 3.3×10^{-7} refractive index unit (RIU) in bulk. A 3D network of SU-8 polymer microfluidics monolithically assembled at the wafer-level was included, ensuring perfect sealing and compact packaging. To overcome some of the drawbacks inherent to interferometric read-outs, a novel all-optical wavelength modulation system has been implemented, providing a linear response and a direct read-out of the phase variation. Sensitivity, specificity and reproducibility of the wavelength modulated BiMW sensor has been demonstrated through the label-free immunodetection of the human hormone hTSH at picomolar level using a reliable biofunctionalization process.

Introduction

One of the main challenges of the 21st century is related to human health, including environment monitoring, food safety and early medical diagnostics. These fields share the common need of detecting very low concentration of analytes or toxins in real-time. Traditional techniques, such as ELISA or RIA tests, suffer from important limitations: laborious sample preparation, the need of bulky instrumentation and slow data processing. Moreover, they often have to be performed by specialized technicians in laboratory environments. To overcome these drawbacks, the implementation of a portable, easy-to-use and highly sensitive biosensor lab-on-a-chip (LOC) for label-free and real-time analysis is mandatory. A LOC must combine, ideally, all the functionalities on a single chip: fluid handling, sample preparation (filtration, homogenization, dilution, *etc.*), target detection and signal processing. During the last few years, the quest for such fast and efficient analytical platforms has attracted the attention of many researchers.[1,2]

When dealing with a biosensor LOC system, the first issue to solve is the choice of the transducer. Even if the validity of electrochemical methods has already been demonstrated for several applications,[3,4] optical detection is generally considered as the most promising method for the development of label-free LOC platforms. In particular, integrated optical (IO) devices are having an increasing impact[5–7] as they offer high sensitivity, mechanical stability, miniaturization and the possibility of mass-production. They also present the advantages inherent to optical read-outs, *i.e.* non-invasive and non-destructive nature, absence of risk of electrical shocks or explosions and immunity to electromagnetic interferences. In addition, IO transducers have a great potential for parallel measurements making multiplexed detection feasible.

Most of the IO sensors are based on the evanescent field detection principle: the biomolecular interaction between the analyte to detect and the corresponding bioreceptor immobilised on the waveguide (WG) surface within the evanescent field region results in a variation of the refractive index of the WG outer medium. This modification affects the effective index of the wave propagating in the WG which can be detected by

[a]*Nanobiosensors and Bioanalytical Applications Group (CIN2) CSIC and CIBER-BBN, Campus UAB, Barcelona, Spain. E-mail: laura.lechuga@cin2.es*
[b]*Institute of Photonic Sciences, ICFO, 08860, Castelldefels, Barcelona, Spain*
[c]*Group of Structural Mechanics and Materials Modelling (GEMM-I3A), University of Zaragoza and CIBER-BBN, Zaragoza, Spain*
[d]*Microelectronics National Center (IMB-CNM) CSIC, Campus UAB, Barcelona, Spain*

† Published as part of a themed issue in collaboration with the III International Workshop on Analytical Miniaturization and NANOtechnologies, Barcelona, 2012.

‡ Electronic supplementary information (ESI) available. See DOI: 10.1039/c2lc40054e

measuring the intensity, the phase, the resonant momentum or the polarization of the output signal. In this detection scheme, there is no need for labelling or prior separation of non-specific components making label-free detection feasible. Among the different IO sensors described in the literature or commercially available, it is worthwhile mentioning those using micro-ring resonators, with a limit of detection (LOD) of 7.6×10^{-7} refractive index unit (RIU) in bulk[8] and 0.3 pg mm^{-2} in mass surface density,[9] grating couplers (LOD: 2.5×10^{-6} RIU and 0.3 pg mm^{-2}),[10] photonic crystals (LOD: 1.6×10^{-4} RIU and 2.1 pg mm^{-2}),[11] Young interferometers (LOD: 6×10^{-8} RIU and 0.02 pg mm^{-2})[12] or Mach-Zehnder interferometers (LOD: 1×10^{-7} RIU and 0.06 pg mm^{-2}).[13] The methodologies used to determine the LOD for each type of sensor can slightly differ from one sensor to another. However, the comparison among the different types of evanescent sensors can be done using the mass surface density because all of them are sensitive to any accumulation of mass on their surface. Therefore, this is an evaluation of their real biosensing capabilities which is not the case when the LOD is expressed as analyte concentration, due to the dependence with the target molecule and its affinity constant.

However, despite the growing interest of the academic and industrial communities, very few stand-alone LOC platforms based on IO sensors have emerged. Indeed, the transit from bulky and complex laboratory equipment to a small, portable and cheap LOC device with low consumption remains a challenge: even if the technologies for each component are mature, their integration into a single platform is complex. The device must be carefully designed since it is not merely the sum of the basic units.

One key issue in the development of LOC devices is the way to bring the sample in contact with the sensing area. The volume of the sample and the flow rate are critical parameters, especially for clinical testing where it is extremely important to reduce the sample volume. Recent technological efforts to combine the fields of photonics and microfluidics have led to the development of optofluidics, in which optical and fluidic systems are integrated together to provide improved functions and performances. The interest in this field is demonstrated by the increasing number of papers and reviews published over the last few years.[14,15]

In the case of IO sensors, the way to couple light into the WG is another critical aspect since an efficient coupling increases the sensitivity of the device through an improved signal-to-noise ratio. Common in-coupling techniques are the end-fired method, the prism coupling and the grating assisted coupling, the last one being the most suitable for future commercial devices as it provides better integration and stability. However, very few publications have demonstrated biosensing capabilities of IO sensors incorporating grating couplers, especially in the visible range. An exception is with the multiplexed ring resonator array integrated with microfluidics and grating couplers developed by Carlborg *et al.*[16] or the grating coupled with a WG interferometer recently optimized by Kozma *et al.*[17]

The biofunctionalization protocol is a third aspect which also plays a crucial role in the biosensor LOC performance as it will guarantee the sensitivity, selectivity, stability and longevity of the biosensor. Enormous efforts are continuously being invested to develop new strategies adapted to a particular application and to each type of silicon-based photonic sensor.[6,18]

Taking into account all of the above described aspects, different attempts have been made to integrate multiplexed IO biosensors into LOC platforms and promising results have been achieved.[19,20] However these systems still require complex read-out laboratory instrumentation, losing the advantages of portability and simplicity. Therefore, the main difficulty when implementing truly LOC devices for point-of-care platforms lies in the incorporation of real "on-chip" detection.

To solve this gap, we present here our latest advances towards the assembly of a LOC platform with "on-chip" detection using a recently developed nanophotonic biosensor, the bimodal waveguide (BiMW) interferometer (Fig. 1a). We have previously reported a limit of detection of 2.5×10^{-7} RIU for this sensor and we have demonstrated the biosensing proof-of-concept of one single sensor by monitoring the biomolecular interaction of the pair BSA/anti-BSA.[21] Due to the excellent performance of a single BiMW sensor, we now aim to integrate it into a complete LOC platform, as shown in Fig. 1b. In this work, our main focus is the complex task of integration of the array of BiMW devices with grating couplers operating at the visible range and with a polymer microfluidic network. We also introduce a novel all-optical modulation technique to improve the optical read-out of the system. In addition, improved surface biofunctionalization protocols have been designed *ad hoc* for high sensitivity, reproducibility and specificity towards the biosensing detection.

In the first part, the working principle and the fabrication processes of the nanometric BiMW transducer will be presented as well as the experimental set-up. Then, the successful

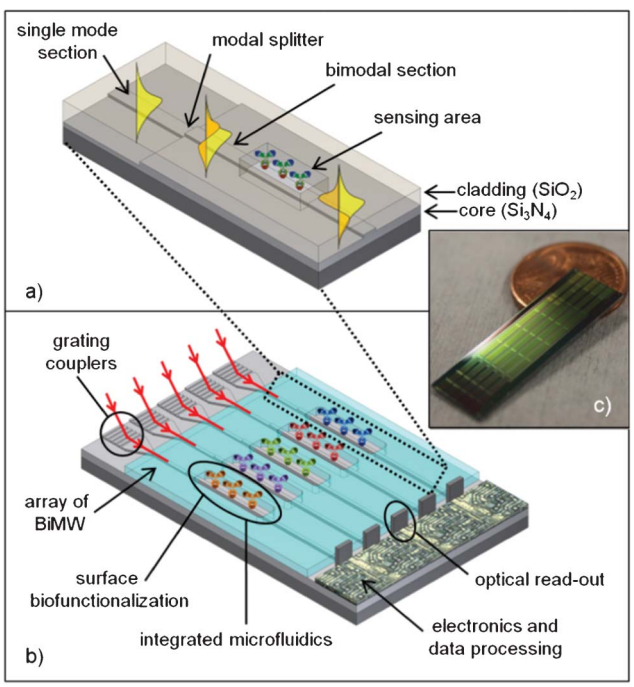

Fig. 1 (a) Scheme of the BiMW interferometer highlighting the distribution of the electromagnetic field in the single mode and the bimodal sections. (b) Scheme of the envisioned LOC platform based on BiMW sensors. (c) Photograph of a chip of 30×10 mm^2 containing 16 BiMW interferometers.

integration of several of the required units of a LOC platform will be demonstrated: (i) nanograting couplers operating at visible range for efficient light in-coupling into the BiMW interferometers, (ii) a novel all-optical wavelength modulation system to ensure linear response and avoid false read-out, (iii) reliable immobilisation protocols at the sensor surface and the immunosensing of the human hormone hTSH at pM level and (iv) a 3D network of SU-8 polymer microfluidics monolithically assembled at the wafer level with the BiMW sensors.

Bimodal waveguide interferometer

Optical transduction principle

In the BiMW sensor the interference of two WG modes (fundamental and first modes) of the same polarization occurs in a straight WG, without the need for a reference arm.[21] The simplicity of this design using only straight WGs is especially attractive for the implementation of LOC platforms.

As depicted in Fig. 1a, the light from a coherent source is first coupled (by end-fire method or *via* a grating coupler) into a rib WG that supports a single transversal mode. After a certain distance, the guided beam reaches a modal splitter that splits the first guided mode in two transversal modes, the fundamental and the first order modes, which are propagating until the output of the chip. A sensor area is defined on the bimodal part of the WG and, as the fundamental and the first order modes have different intensity distributions at the core-cladding interface, the interference pattern is a function of the refractive index in the sensing region. In this scheme, there is no need for Y-junctions facilitating the device fabrication as compared to other interferometric configurations. Moreover, the interference pattern does not depend on the light intensity or on coupling variations, which are important drawbacks when using Mach–Zehnder or Young interferometers.

Regarding multiplexing, the small footprint of the BiMW interferometer allows the integration of a large amount of sensing elements within a single chip. For instance, Fig. 1c shows a chip of 30 × 10 mm^2 containing 16 BiMW distributed as four groups of four, therefore up to 30 interferometers could be easily integrated in such chips.

Optical chip

To optimize the sensor design, calculations and simulations were previously carried out as described elsewhere.[21] According to the modelization, lithographic masks and devices were fabricated using standard microelectronics technology. The bottom cladding layer consists of a 2 μm thick, thermally grown silicon dioxide layer (n_{SiO_2} = 1.46 at 658 nm) deposited on a silicon wafer. Then, a 350 nm thick core layer of silicon nitride ($n_{Si_3N_4}$ = 2.00 at 658 nm) is deposited by LPCVD. The thickness of the single mode section is reduced to 150 nm using conventional photolithography and dry etching processes. Once the two different modal sections are defined, the nanometric rib structure of the WG (4 μm in width and less than 1.5 nm in height) is generated by BHF etching through a photoresist mask patterned by photolithography. The top cladding layer, a silicon dioxide layer (n_{SiO_2} = 1.48 at 658 nm), is then deposited by PECVD. The final wet etching step defines the sensing window (15 × 0.05 mm^2) and the 2 mm long grating window.

The choice of a standard fabrication process offers important advantages such as robustness, reliability and potential for mass production with consequent reduction of costs. In addition, the integration of light sources, photodetectors and CMOS processing electronics into the LOC platform would be facilitated if needed.

Experimental set-up and procedures

To control the temperature of the chip, a Peltier device, composed of a copper base and a thermo-electric element (TEC 3–2.5, Thorlabs) connected to a temperature controller (TED 200C, Thorlabs), was integrated into a PMMA holder. The whole structure is placed on a XYZ translation stage (NanoMax, Thorlabs, travel range: 4 mm, resolution: 1 μm).

For light coupling into the chip, two different methods have been used: end-fire coupling and grating assisted coupling. In the end-fire method, light from a high-power laser diode (ML101J27, Mitsubishi, λ_0 = 658 nm, 120 mW) is coupled into the WG using a ×40 microscope objective (Fig. S1a, ESI‡). For the grating coupler method, a fiber pigtailed laser diode (LPS-660-FC, Thorlabs, λ_0 = 658 nm, 7.5 mW) is mounted on a rotation stage placed above the chip to control the incidence angle of the focused beam (Fig. S1b, ESI‡). In both cases, TE polarization is employed.

The interference pattern produced at the output of the BiMW is directly monitored by a two sectional photodiode (S5870, Hamamatsu), each section being connected to a current amplifier (PDA 200C, Thorlabs). The currents generated in the upper and lower part of the photodetector, I_{up} and I_{down} respectively, are functions of the interference pattern. To quantify the variation of this pattern, we define the sensor signal S as

$$S(\%) = \frac{I_{up} - I_{down}}{I_{up} + I_{down}} \times 100 \quad (1)$$

When a variation of the phase difference $\Delta\varphi_S$ is induced between the two guided modes, for instance by varying the refractive index in the sensing area, it results into an intensity variation of S that can be expressed as:

$$S(t) \propto \cos(\Delta\varphi_S(t)) \quad (2)$$

As it can be deduced from eqn (2), the output of the BiMW device is periodic with respect to the phase changes induced in the sensing area.

The microfluidic header used for preliminary measurements is a PDMS flow cell encapsulated in a PMMA housing to provide connections to the exterior. The microfluidic header has four independent channels of 3 μl each, one on top of each of the four groups of interferometers.

Prior to biomeasurements, the sensitivity of the device is evaluated measuring the phase changes $\Delta\varphi$ induced by refractive index variations Δn in the sensing area. Different concentrations of HCl (from 0.03 to 0.5 M) are injected using a syringe pump with running water (milli-Q grade) as buffer. The refractive indices of the solutions have been previously measured with an

ABBE refractometer (Optic Ivymen System). Table 1 reports the absolute refractive indices and the index difference induced in the sensing area considering milli-Q water (n = 1.3329) as the buffer.

Important features to characterize the sensor response are the phase resolution, the sensitivity and the LOD. The phase resolution ($\Delta\varphi_{min}$) is considered as three times the noise-to-signal ratio. The sensitivity of the sensor is defined as $S_{sensor} = \Delta\varphi/\Delta n$ for bulk measurements and as $S_{sensor} = \Delta\varphi/$[anti-hTSH] for the biosensing interactions. In both cases, the sensitivity S_{sensor} corresponds to the slope of the calibration curve. For refractive index variation, the LOD Δn_{min} is given by $\Delta n_{min} = \Delta\varphi_{min}/S_{sensor}$ and by $[\text{anti-hTSH}]_{min} = \Delta\varphi_{min}/S_{sensor}$ for the anti-hTSH concentration.

We have previously reported a LOD of 2.5×10^{-7} RIU using end-fire coupling from a HeNe laser (λ_0 = 633 nm).[21] This previous result will be used as a reference to compare and estimate the performance of the BiMW device while it is progressively integrated with the required elements of the LOC platform.

Implementation of the lab-on-a-chip platform

Grating couplers

The coupling of light into a WG is an important issue to solve when dealing with LOC based on IO sensors. Our solution is to integrate grating couplers at the input of the BiMW interferometers, making feasible better integration, stability and alignment tolerance when compared to the traditional end-fire method. Moreover, when coupling light with gratings, no polishing of the chip edges is required. To our knowledge, the integration of grating couplers with optical biosensors for wavelengths in the visible range has not been previously reported.

Due to the sub-micronic cross-section of the WG and to the operating wavelength (λ = 658 nm), the grating length cannot exceed 100 μm with a sub-micronic period which makes it suitable for high scale integration. To increase the coupling efficiency, the grating is associated to a tapered WG with an initial width of 20 μm that linearly reduces until reaching the BiMW width (4 μm). The resonant coupling between the guided TE mode and the grating is obtained when the following phase matching condition is verified:

$$\sin\theta = n_{eff} + m\frac{\lambda}{\Lambda} \quad (3)$$

with θ the incidence angle, n_{eff} the effective index of the guided mode in the BiMW (here n_{eff} = 1.677499), m the diffraction order (here $m = -1$), λ the wavelength and Λ the grating period.

Table 1 Refractive indices of the HCl solutions used for calibration

Solutions	n	Δn
HCl 0.03 M	1.3332 ± 0.0001	$(3 \pm 2) \times 10^{-4}$
HCl 0.05 M	1.3334 ± 0.0001	$(5 \pm 2) \times 10^{-4}$
HCl 0.1 M	1.3338 ± 0.0001	$(9 \pm 2) \times 10^{-4}$
HCl 0.2 M	1.3348 ± 0.0001	$(1.9 \pm 0.2) \times 10^{-3}$
HCl 0.3 M	1.3357 ± 0.0001	$(2.8 \pm 0.2) \times 10^{-3}$
HCl 0.4 M	1.3366 ± 0.0001	$(3.7 \pm 0.2) \times 10^{-3}$
HCl 0.5 M	1.3376 ± 0.0001	$(4.7 \pm 0.2) \times 10^{-3}$

Eqn (3) is used to design gratings with incidence angles ranging from 5° to 15°. This range of angles enables an efficient coupling but, above all, it is an important requirement for the implementation of the complete LOC platform where the different units have to be integrated all together in a minimum of space without disturbing each other.

Taking into account the above considerations, the gratings are directly written onto the Si_3N_4 WG by electron beam lithography and reactive ion etching with a period of 450 nm, a duty cycle of 0.5 and a depth of 50 nm. The set-up shown in Fig. S1b (ESI‡) is used to excite the grating. An example of light coupled into a BiMW *via* a grating is shown in Fig. S2 ($\theta = 9°50'$) (ESI‡).

The sensitivity of the BiMW interferometer integrated with grating couplers is evaluated by carrying out a calibration curve with the set of solutions of HCl (Table 1). Fig. 2a shows the response of the system to an injection of a solution of HCl 0.2 M with milli-Q water as running buffer ($\Delta n = 1.9 \times 10^{-3}$). The phase starts at a constant level, corresponding to the running water, then oscillates when the HCl solution reaches the sensing area of the BiMW and finally stabilises. The total phase difference $\Delta\varphi$ equivalent to this change of index Δn is estimated taking into account that an entire oscillation is equivalent to a $\Delta\varphi$ of 2π. Here, the total phase difference for $\Delta n = 1.9 \times 10^{-3}$ has been estimated to $3.89 \times 2\pi$ rad. The same methodology has been applied to the other solutions and the resulting calibration curve is plotted in Fig. 2b. A linear fit of the experimental data gives a sensitivity of $S_{sensor} = 2000 \times 2\pi$ rad/RIU, with R^2 = 0.999. As the noise-to-signal ratio of the system is $2.2 \times 10^{-4} \times 2\pi$ rad, the phase resolution of the sensor is estimated to be $6.6 \times 10^{-4} \times 2\pi$ rad, rendering in a LOD of 3.3×10^{-7} RIU. This LOD, obtained with a cheap and easily integrated laser diode, is comparable to the one demonstrated in our previous study using a HeNe laser and end-fire coupling.[21] This strongly supports the adoption of the grating coupler method for the achievement of a truly portable and sensitive LOC platform.

It should be noted that in the case of BiMW interferometers, gratings for light out-coupling are not needed as we opted for a direct monitoring of the signal with a two sectional photodiode directly placed at the WG output.

All-optical phase modulation

An important drawback of interferometric sensors comes from the periodic nature of the output signal which can give rise to

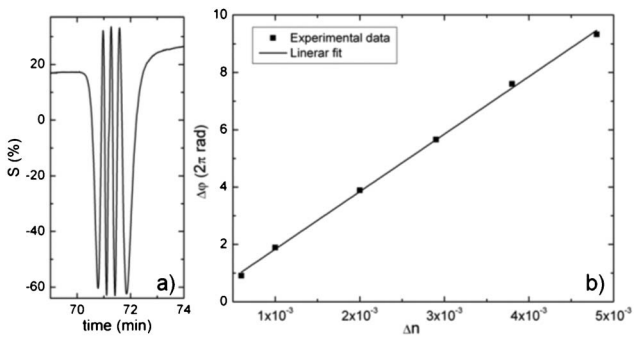

Fig. 2 (a) Sensor response in the case of an index change of $\Delta n = 1.9 \times 10^{-3}$ and (b) calibration curve obtained with a BiMW excited *via* a grating coupler (TE polarization, $\theta = 9°50'$).

wrong or ambiguous interpretations. This problem can be solved by implementing a phase modulation system[22] based for instance on electro-optical,[22] acousto-optical[23] or magneto-optical[24] working principles. However these techniques generally involve non-standard CMOS materials and rely on complex read-out equipment which clearly impedes their integration into LOC platform. To overcome these difficulties, we have recently proposed a new all-optical modulation approach which provides a real-time and direct read-out of the phase variation without additional fabrication processes and instrumentation.[25] We have expanded this idea to the BiMW sensors.

In this modulation scheme, the phase difference between the two modes propagating in the BiMW is controlled by tuning the input wavelength of the guided light by a few nanometers. According to our calculations, a wavelength variation of 2 nm is enough to induce a shift of 2π rad between the two modes. This wavelength variation is easily obtained by taking advantage of a drawback of the commercial Fabry–Perot laser diodes, *i.e.* the dependence of their emission wavelength with the driving current. Therefore, by applying a sinusoidal variation to the laser driving current, it is possible to induce a periodic phase change in the WG. As a consequence of this periodical change, the sensor output defined by eqn (2) is now expressed by:

$$S(t) \propto \cos(\Delta\varphi_S(t) + \mu_M \sin(\omega t)) \quad (4)$$

where μ_M is the amplitude and ω the frequency of modulation. A fast fourier transform deconvolution of the output signal, performed in real-time with a labview application, gives a direct read-out of the phase variation.[25]

To implement this method, we used the end-fire coupling (Fig. S1a, ESI‡). The 2 nm wavelength shift was obtained with the laser diode ML101J27 (Mitsubishi). Fig. 3a shows the real-time sensor response during the injection of a solution of HCl 0.2 M with milli-Q water as running buffer ($\Delta n = 1.9 \times 10^{-3}$). The phase starts at a constant level, increases when the HCl solution reaches the sensing area and then stabilises. The difference between the two constant levels is the phase difference corresponding to the index variation in the sensing area (here, $\Delta\varphi = 4.17 \times 2\pi$ rad). With this approach, the phase information is not deduced anymore from the variation of the interference pattern (as the one shown in Fig. 2a) but it is directly monitored,

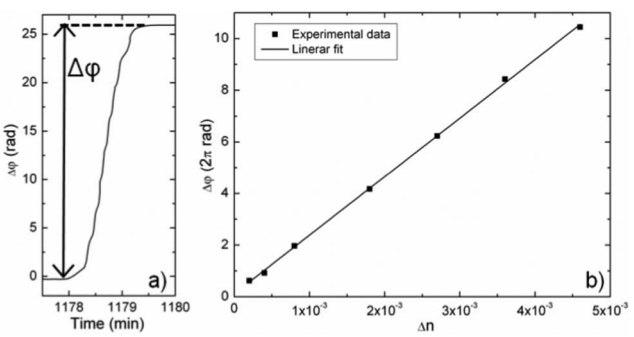

Fig. 3 (a) Real-time monitoring of the phase variation due to a change of $\Delta n = 1.9 \times 10^{-3}$ and (b) calibration curve of the wavelength modulated BiMW (TE polarization, laser driving current: (143 ± 51) mA, modulation frequency: 215 Hz) for different refractive indexes changes.

solving all the problems of false read-out responses arising from interferometric signals. In addition, this detection scheme provides a theoretically infinite dynamic range of phase variation.

The phase changes for the complete set of HCl solutions have been evaluated in the same way. As a result, Fig. 3b shows the calibration curve obtained with a wavelength modulated BiMW (TE polarization, laser driving current: (143 ± 51) mA, modulation frequency: 215 Hz). A linear fit results in a sensitivity of $S_{sensor} = 2300 \times 2\pi$ rad/RIU, with $R^2 = 0.999$. Taking into account a standard deviation of the system of $3.2 \times 10^{-4} \times 2\pi$ rad, the phase resolution of the sensor is estimated to be $9.6 \times 10^{-4} \times 2\pi$ rad, with a LOD of 4.2×10^{-7} RIU. Again, this LOD achieved using cheap, compact and easily integrated laser diode is comparable to our previous results with bulky HeNe laser.[21] This, in addition to the direct phase read-out, clearly promotes the adoption of the all-optical wavelength modulation approach for the implementation of a LOC device.

Biofunctionalization and biosensing evaluation of the wavelength modulated BiMW

The biofunctionalization protocol plays a crucial role in the biosensor LOC performance as the immobilisation process should guarantee an efficient coverage of the transducer surface and ensure sensitivity, selectivity and stability of the biosensor. Different immobilisation strategies can be employed according to the selected application, *i.e.* to the nature of the bioreceptor to be immobilised. However, one of the most reliable strategies is the covalent binding through one of the chemical groups of the molecules.[6] In particular, for proteins the preferred options are amino, carboxylic or thiol groups. To provide the sensor area with functional groups allowing covalent binding, silane molecules are extensively used.

The implementation of a suitable silanization method involves the optimization of different steps, such as the activation of the silicon surface by oxidation processes and the covalent anchorage of the silane molecule. In order to covalently attach proteins on the BiMW transducer, we decided to use a carboxyethylsilanetriol sodium salt silane (CTES, abcr). The CTES allows the formation of a stable and homogeneous silane monolayer on the silicon nitrate surface with carboxylic end-groups. Due to its short alkyl chain (6 Å) and the hydrophilicity of the functional carboxylic group, CTES is a water soluble silane, making this functionalization strategy especially attractive for biosensing. The achievement of an enduring peptidic bond between the carboxylic groups present on the transducer surface and amino groups of the proteins is obtained by the use of 1-ethyl-3-[3-dimethylaminopropyl] carbodiimide hydrochloride (EDC, Sigma-Aldrich) and *N*-hydroxysulfosuccinimide (NHS, Sigma-Aldrich).

We have selected as a clinical application the detection of the human thyroid stimulating hormone (hTSH), secreted by the anterior pituitary gland. The determination of low concentrations of hTSH is of clinical importance in the case of hyperthyroid syndromes such as thyroid adenoma, nodular goiter or the autoimmune disorder Graves' disease for which hTSH serum levels are below normal ones (normal concentration is considered to be between 2–20 pM). To detect such low levels,

a competitive immunoassay was carried out with the wavelength modulated BiMW. In a competitive assay, the antigen to detect (here the hTSH) is immobilised on the sensor surface. Afterwards, an antibody solution of an appropriate concentration is incubated with the sample. The hormone concentration is then detected in an indirect way, by means of the signal obtained by the immunoreaction of the free antibodies in the solution with the immobilised hormones. This procedure implies more time and reagent consumption than direct methods but it allows the reuse of the bioreceptor surface for many cycles thanks to regeneration solutions. In direct methods, the antibodies are immobilised on the sensor surface but after the biomolecular interaction, the use of regeneration solutions can easily denaturalize them. In a competitive immunoassay, several detections can be performed using the same bioreceptor layer, reducing the total cost and duration when a complete analytical study is required.

In order to monitor in real time the interferometric signals obtained by the different steps of the biofunctionalization procedure, the processes are done *in situ*, with the BiMW chip mounted with the microfluidic header on the experimental set up (Fig. S1a, ESI‡). During the entire functionalization procedure, water flow is maintained at a constant rate of 10 μl min^{-1} and the different solutions are injected in volumes of 250 μl. The generation of reactive silanol groups on the sensor surface is achieved by flowing a 20% nitric acid solution through the microfluidic channels. Three consecutive injections of the oxidizing solution were required to stabilise the interferometric signal. Then, a CTES solution at a concentration of 1% in water is employed to create a well-packed monolayer of silane molecules. The ended carboxylic groups of the silane are activated afterwards through EDC/NHS (0.2 M/0.05 M) chemistry. The hTSH is then immobilised by covalent bonding by supplying a 10 μg ml^{-1} solution of hTSH in phosphate buffer saline (PBS, 10 mM phosphate, 2.9 mM KCl, 137 mM NaCl, pH 7.4, Sigma-Aldrich). The hTSH solution is injected twice, to ensure total protein coverage of the surface. Finally, a solution of ethanolamine (1 M, pH 8.5, Sigma-Aldrich) is injected in order to react with activated carboxylic groups, protecting the surface against unspecific adsorption. The buffer is then changed to PBS that is maintained during all the experiments at a constant rate of 20 μl min^{-1}. Different solutions of the specific monoclonal antibody of hTSH (anti-hTSH) are injected, with concentrations ranging from 0.5 to 5 μg ml^{-1}. Regeneration of the biosensing surface is achieved by an injection of an HCl solution (20 mM). The resulting calibration curve, expressed as the phase variation as function of the anti-hTSH concentrations, is shown Fig. 4a. A linear fit results in a sensitivity of S_{sensor} = 0.21 × 2π rad (μg ml^{-1})$^{-1}$, with R^2 = 0.994. Taking into account a standard deviation of the system of 1.2 × 10^{-3} × 2π rad, the phase resolution of the sensor is estimated to be 3.6 × 10^{-3} × 2π rad. This corresponds to a LOD of 17 ng ml^{-1}, which means a surface coverage of 0.38 pg mm^{-2}.

Highly specific signals have been obtained as can be deduced from the control experiment presented in Fig. 4b. The injection of a concentration of 5 μg ml^{-1} of anti-hTSH produces a phase variation of 1.22 × 2π rad, while an injection of 5 μg ml^{-1} of the antibody against human growth hormone (anti-hGH), the control antibody, does not induce significant phase variation, demonstrating the high selectivity of the immunoassay.

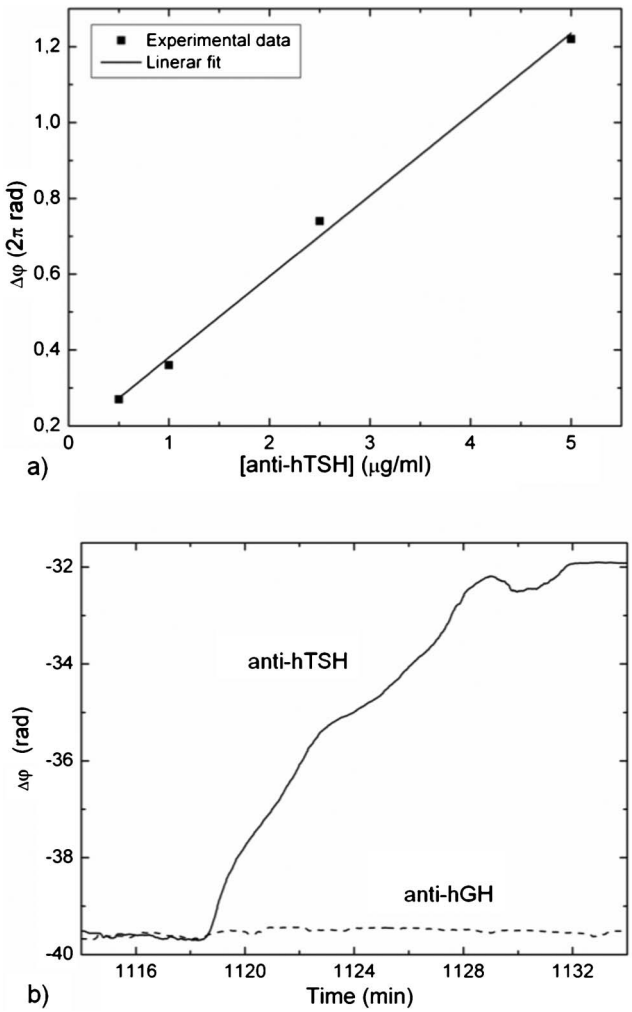

Fig. 4 (a) Calibration curve for the detection of different concentrations of anti-hTSH. (b) Control experiment: real-time monitoring of the phase variation for the detection of anti-hTSH 5 μg ml^{-1} and of anti-hGH 5 μg ml^{-1} employed as control. Results obtained with a wavelength modulated BiMW sensor (TE polarization, laser driving current: (143 ± 51) mA, modulation frequency: 215 Hz).

According to the above results, a fixed concentration of anti-hTSH of 1 μg ml^{-1} has been chosen to perform a competitive immunoassay. A 1 μg ml^{-1} solution of anti-hTSH is thus incubated with a 1 ng ml^{-1} hTSH solution and injected on the sensor surface. The results are shown in Fig. 5: the injection of 1 μg ml^{-1} of anti-hTSH induces a phase difference of 0.31 × 2π rad while the injection of the incubated solution of 1 μg ml^{-1} of anti-hTSH with 1 ng ml^{-1} of hTSH produces a phase difference of only 0.14 × 2π rad. This detection corresponds to a concentration of hTSH of 20 pM. However, given the significant phase difference between the two signals, lower concentrations should easily be detected once the competitive assay protocols *in situ* is further optimized.

Regarding reproducibility, the detection of anti-hTSH 1 μg ml^{-1} has been repeated three times. The sensor response was similar for the three evaluations: a standard deviation of 0.03 × 2π rad was

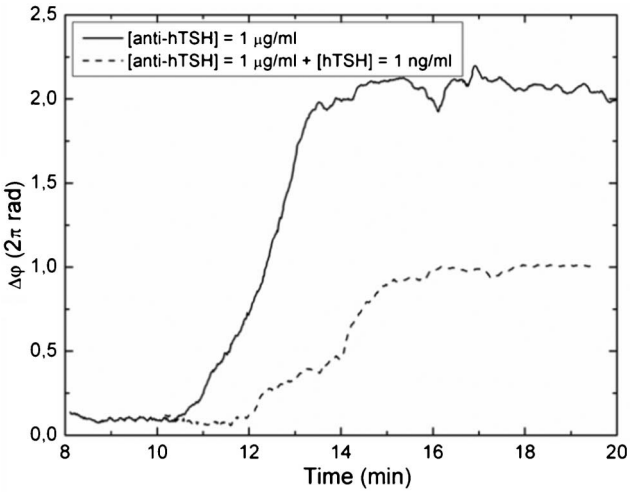

Fig. 5 Competitive assay: real-time monitoring of the phase variation for the detection of 1 μg ml^{-1} of anti-hTSH (solid line) and for the indirect detection of hTSH (1 μg ml^{-1} of anti-hTSH + 1 ng ml^{-1} of hTSH) (dashed line).

found for a mean value of 0.29 × 2π rad. These results, obtained with a new wavelength modulated BiMW interferometer, are promising as they clearly demonstrate high sensitivity, reproducibility and specificity.

Microfluidics and packaging

In order to integrate a dedicated microchannel on each of the 16 sensors contained in each single chip, SU-8 based microfluidic technology was applied.[26,27] Fig. S3 (ESI‡) includes the schematic process flow used for the fabrication of the microfluidics devices. The process starts with the spinning of a 20 μm thick SU-8 layer, followed by a soft-bake step (7 min at 90 °C). Then, another layer is spun and soft-baked in the same way to end up with a 50 μm thick layer (Fig. S3a‡). The increased thickness from the expected 40 μm thick layer is caused by the difference in surface friction. While the first SU-8 layer is spun on top of silicon oxide, the second SU-8 layer is spun on top of SU-8 material, increasing the final thickness. Once the final 50 μm thick layer is obtained, an exposure of 140 mJ ultraviolet light (365 nm wavelength) is applied using a mask which defines 100 μm wide microchannels. Then, a post-bake step is performed (4 min at 95 °C) followed by a gentle development for 4 min to remove the unexposed SU-8 (Fig. S3b‡). At this point, open microchannels are defined on top of every WG present on the chip. Since any debris deposited on top of the silicon nitride will dramatically decrease the resolution of the sensor, an oxygen plasma step was included as an extra cleaning step (100 watt and 50 sccm oxygen flow during 1 h). The wafer was then measured by AFM to confirm that the silicon nitride sensing areas were completely SU-8 free.

To close the microchannels, another wafer with kapton on top was processed to carry a 40 μm thick SU-8 layer (Fig. S3c‡). This layer is meant to be the cover of the channels with the inlets and outlets already patterned by photolithography (Fig. S3d‡). After the alignment of both wafers, a bonding step using a pressure of 3 bars at 90 °C during 30 min (Fig. S3e‡) was performed. The selected exposure and post bake conditions in combination with the chosen pressure and temperature values for the bonding step, render in a perfect bonding with no deformation of the microchannel dimensions.[28,29] The kapton wafer was then manually released from the silicon wafer thanks to its low adhesion to SU-8 (Fig. S3f‡). As a result, the microchannels were finally closed with inlets and outlets accessible from the top of the wafer (Fig. 6a).

Due to the high density of microchannels present on the chip, the device and the packaging were designed to use one dedicated inlet for each microchannel (Fig. 6b), but a common outlet for every four sensors (Fig. 6c). In this way, only 20 fluidic connections between the chip and the packaging were required to handle the device (instead of 32). As a result, the microfluidic connection between the outside and the sensor was done by the use of standard fluidic connectors and O-rings, ensuring a perfect sealing (Fig. 6d).

Conclusions and perspectives

We are implementing a sensitive, affordable, hand-held and portable device for point-of-care diagnosis of relevant analytes. Our LOC platform is based on an innovative BiMW interferometer which has already shown its capabilities for sensitive, label-free and real-time biosensing. In contrast to most IO biosensors, the design of our interferometer is simple, allowing easy fabrication processes and integration.

Light in-coupling into the nano-interferometers using grating couplers has been achieved, leading to a limit of detection of 3.3 × 10^{-7} RIU in bulk. A wavelength modulation system has been implemented in order to simplify data read-out and to solve some of the problems inherent to periodic signals. In addition, a versatile silanization method for surface biofunctionalization has been implemented and the detection of 20 pM of hTSH has been successfully demonstrated, showing high sensitivity, reproducibility and specificity. Regarding the microfluidic platform, a 3D microchannel network in SU-8 was fabricated at the wafer-level, ensuring a perfect sealing.

Our system presents a high degree of integration as submicronic structures are employed in combination with compact laser diodes and simple read-out instrumentation. An additional advantage of our device lies in the use of standard silicon

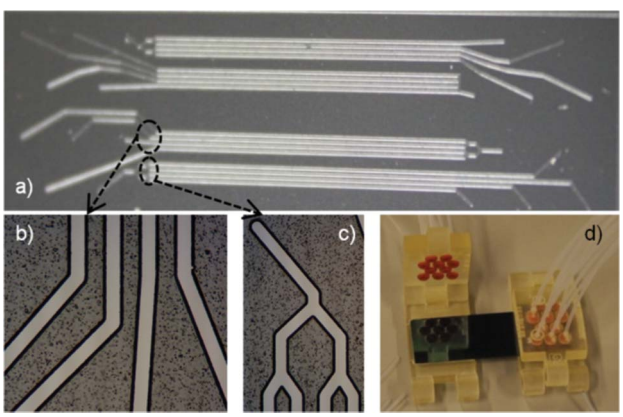

Fig. 6 Optical images of the 3D SU-8 microfluidic network: (a) BiMW chip with 16 channels, one on top of each sensor, (b) individual inlets of 4 sensors (c) common outlet of 4 sensors and (d) final encapsulation.

technologies together with polymer material processing, which could allow mass production with consequent reduction of costs.

Work is in progress in order to evaluate the surface sensing limit of detection of the wavelength modulated BiMW integrated with the grating couplers and the SU-8 microfluidic platform. Moreover, BiMW interferometers are currently being implemented in a multiplexed configuration, taking advantage of the individual inlet of the microchannel network to functionalize individually each BiMW sensor. The final prototype will incorporate the individual components presented here, plus commercial laser diodes, photodetectors, control electronics, firmware and software, sensor read-out algorithms and a user interface.

Acknowledgements

This work was partially developed using the micro and nano fabrication capabilities of the ICTS/clean room from the IMB-CNM (CSIC) and has been sponsored by Fundación M. Botín. The authors acknowledge A. García Castaño for the fabrication of the PMMA microfluidic header. S. Dante acknowledges the "Programa de Formación de Profesorado Universitario (FPU)" of the "Ministerio de Educación" of Spain.

References

1 C. D. Chin, V. Linder and S. K. Sia, *Lab Chip*, 2007, **7**, 41–57.
2 F. S. Ligler, *Anal. Chim. Acta.*, 2009, **81**, 519–526.
3 M. A. Schwarz and P. C. Hauser, *Lab Chip*, 2001, **1**, 1–6.
4 J. Wang, *Biosens. Bioelectron.*, 2006, **21**, 1887–1892.
5 P. V. Lambeck, *Meas. Sci. Technol.*, 2006, **17**, R93–R116.
6 M. C. Estevez, M. Alvarez and L. M. Lechuga, *Laser Photonics Rev.*, 2011, DOI: 10.1002/lpor.201100025.
7 A. Kussrow, C. S. Enders and D. J. Bornhop, *Anal. Chem.*, 2012, **84**, 779–792.
8 M. Iqbal, M. A. Gleeson, B. Spaugh, F. Tybor, W. G. Gunn, M. Hochberg, T. Baehr-Jones, R. C. Bailey and L. C. Gunn, *IEEE J. Sel. Top. Quantum Electron.*, 2010, **16**, 654–661.
9 D. X. Xu, M. Vachon, A. Densmore, R. Ma, A. Delâge, S. Janz, J. Lapointe, Y. Li, G. Lopinski, D. Zhang, Q. Y. Liu, P. Cheben and J. H. Schmid, *Opt. Lett.*, 2010, **35**, 2771–2773.
10 K. Cottier, M. Wiki, G. Voirin, H. Gao and R. E. Kunz, *Sens. Actuators, B*, 2003, **91**, 241–251.
11 J. García-Rupérez, V. Toccafondo, M. J. Bañuls, J. G. Castelló, A. Griol, S. Peransi-Llopis and Á. Maquieira, *Opt. Express*, 2010, **18**, 24276–24286.
12 A. Ymeti, J. Greve, P. V. Lambeck, R. Wijn, R. G. Heideman and J. S. Kanger, *Appl. Opt.*, 2005, **44**, 3409–3412.
13 K. E. Zinoviev, L. G. Carrascosa, J. Sánchez del Río, B. Sepúlveda, C. Domínguez and L. M. Lechuga, *Adv. Opt. Technol.*, 2008, **Article ID 383927**, 1–6.
14 F. B. Myers and L. P. Lee, *Lab Chip*, 2008, **8**, 2015–2031.
15 X. Fan and I. M. White, *Nat. Photonics*, 2011, **5**, 591–597.
16 C. F. Carlborg, K. B. Gylfason, A. Kazmierczak, F. Dortu, M. J. Banuls Polo, A. Maquieira Catala, G. M. Kresbach, H. Sohlstrom, T. Moh, L. Vivien, J. Popplewell, G. Ronan, C. A. Barrios, G. Stemme and W. van der Wijngaart, *Lab Chip*, 2010, **10**, 281–290.
17 P. Kozma, A. Hámori, S. Kurunczi, K. Cottier and R. Horvath, *Sens. Actuators, B*, 2011, **155**, 446–450.
18 J. T. Kirk, G. E. Fridley, J. W. Chamberlain, E. D. Christensen, M. Hochberg and D. M. Ratner, *Lab Chip*, 2011, **11**, 1372–1377.
19 G. Suarez, Y.-H. Jin, J. Auerswald, S. Berchtold, H. F. Knapp, J.-M. Diserens, Y. Leterrier, J.-A. E. Manson and G. Voirin, *Lab Chip*, 2009, **9**, 1625–1630.
20 A. Crespi, Y. Gu, B. Ngamsom, H. J. W. M. Hoekstra, C. Dongre, M. Pollnau, R. Ramponi, H. H. van den Vlekkert, P. Watts, G. Cerullo and R. Osellame, *Lab Chip*, 2010, **10**, 1167–1173.
21 K. E. Zinoviev, A. B. González-Guerrero, C. Domínguez and L. M. Lechuga, *J. Lightwave Technol.*, 2011, **29**, 1926–1930.
22 R. G. Heideman and P. V. Lambeck, *Sens. Actuators, B*, 1999, **61**, 100–127.
23 M. B. Duhring and O. Sigmund, *J. Appl. Phys.*, 2009, **105**, 083529.
24 B. Sepúlveda, G. Armelles and L. M. Lechuga, *Sens. Actuators, A*, 2007, **134**, 339–347.
25 S. Dante, D. Duval, B. Sepúlveda, A. B. González-Guerrero, J. R. Sendra and L. M. Lechuga, *Opt. Express*, 2012, **20**, 7195–7205.
26 M. Castaño-Álvarez, M. T. Fernández-Abedul, A. Costa-García, M. Agirregabiria, L. J. Fernández, J. M. Ruano-López and B. Barredo-Presa, *Talanta*, 2009, **80**, 24–30.
27 R. Vilares, C. Hunter, I. Ugarte, I. Aranburu, J. Berganzo, J. Elizalde and L. J. Fernandez, *Sens. Actuators, B*, 2010, **147**, 411–417.
28 F. J. Blanco, M. Agirregabiria, J. Berganzo, K. Mayora, J. Elizalde, A. Calle, C. Dominguez and L. M. Lechuga, *J. Micromech. Microeng.*, 2006, **16**, 1006–1016.
29 M. T. Arroyo, L. J. Fernández, M. Agirregabiria, N. Ibañez, J. Aurrekoetxea and F. J. Blanco, *J. Micromech. Microeng.*, 2007, **17**, 1289–1298.